ADVANCED FUNCTIONAL MATERIALS
www.afm-journal.de

Strain-Modulated Ferromagnetism at an Intrinsic van der Waals Heterojunction

*Ryuji Fujita, Gautam Gurung, Mohamad-Assaad Mawass, Alevtina Smekhova, Florian Kronast, Alexander Kang-Jun Toh, Anjan Soumyanarayanan, Pin Ho, Angadjit Singh, Emily Heppell, Dirk Backes, Francesco Maccherozzi, Kenji Watanabe, Takashi Taniguchi, Daniel A. Mayoh, Geetha Balakrishnan, Gerrit van der Laan, and Thorsten Hesjedal**

The van der Waals interaction enables atomically thin layers of exfoliated 2D materials to be interfaced in heterostructures with relaxed epitaxy conditions, however, the ability to exfoliate and freely stack layers without any strain or structural modification is by no means ubiquitous. In this work, the piezoelectricity of the exfoliated van der Waals piezoelectric α-In_2Se_3 is utilized to modify the magnetic properties of exfoliated Fe_3GeTe_2, a van der Waals ferromagnet, resulting in increased domain wall density, reductions in the transition temperature ranging from 5 to 20 K, and an increase in the magnetic coercivity. Structural modifications at the atomic level are corroborated by a comparison to a graphite/α-In_2Se_3 heterostructure, for which a decrease in the Tuinstra-Koenig ratio is found. Magnetostrictive ferromagnetic domains are also observed, which may contribute to the enhanced magnetic coercivity. Density functional theory calculations and atomistic spin dynamic simulations show that the Fe_3GeTe_2 layer is compressively strained by 0.4%, reducing the exchange stiffness and magnetic anisotropy. The incorporation of α-In_2Se_3 may be a general strategy to electrostatically strain interfaces within the paradigm of hexagonal boron nitride-encapsulated heterostructures, for which the atomic flatness is both an intrinsic property and paramount requirement for 2D van der Waals heterojunctions.

1. Introduction

Bulk magnetic van der Waals (vdW) materials can be cleaved down to atomically thin 2D sheets, which often display emergent magnetic behavior such as layer-dependent (anti)ferromagnetism[1] and magnetic skyrmions.[2] More generally, the 2D properties in the atomically thin limit manifest due to reduced out-of-plane (OOP) exchange interaction $J_\perp$,[3] changes in the lattice symmetry,[4] or interfacial coupling.[5]

Although $J_\perp$ can be readily tuned via the thickness,[6] the modification of the in-plane (IP) exchange interaction, $J_\parallel$, is more challenging, but would allow for the study of emergent magnetic ground states, such as the Kitaev spin liquid in strained monolayer $CrSiTe_3$.[7] Strain enhancement of technologically relevant parameters including magnetic coercivity (H_c) and the Curie temperature (T_C) in VI_3[8] and Fe_3GeTe_2[9,10] have already been experimentally demonstrated.

Epitaxy plays a limited role in mechanically exfoliated 2D materials due to the

R. Fujita, G. Gurung, A. Singh, E. Heppell, T. Hesjedal
Clarendon Laboratory
Department of Physics
University of Oxford
Parks Road, Oxford OX1 3PU, UK
E-mail: Thorsten.Hesjedal@physics.ox.ac.uk

The ORCID identification number(s) for the author(s) of this article can be found under https://doi.org/10.1002/adfm.202400552

[+]Present address: Department of Interface Science, Fritz Haber Institute of the Max Planck Society, Berlin Germany

DOI: 10.1002/adfm.202400552

G. Gurung
Trinity College
University of Oxford
Oxford OX1 3BH, UK

M.-A. Mawass[+], A. Smekhova, F. Kronast
Helmholtz-Zentrum Berlin für Materialien und Energie
Albert-Einstein-Strasse 15, 12489 Berlin, Germany

A. K.-J. Toh, A. Soumyanarayanan, P. Ho
Institute of Materials Research and Engineering (IMRE),Agency for Science, Technology and Research (A*STAR)
2 Fusionopolis Way, Innovis #08-03, Singapore 138634, Singapore

A. Soumyanarayanan
Department of Physics
National University of Singapore
2 Science Drive 3, Singapore 117551, Singapore

weak vdW interaction and the chalcogen termination of the vdW lattice along the *c* axis, meaning that atomically thin layers of vdW materials can be sequentially stacked on top of one another, and at varying twist angles.[11] In such atomically sharp vdW heterostructures, optoelectronic mechanisms,[12] spin-orbit interaction,[13] or moiré lattices[14] can be found at the interface. An outstanding question is whether it is still possible to induce strain within the confines of an atomically flat environment, afforded by hexagonal boron nitride (hBN) encapsulation. Although it may seem natural to assume that any arbitrary combination of vdW materials forms an atomically smooth heterojunction free of strain-induced structural distortions, exceptions exist.[15,16] In 2D moiré heterostructures synthesized with the "tear and stack" method,[17] strain fields form, which are commensurate with the moiré periodicity.[18–20] In this regard, the class of vdW piezoelectrics may offer methods of intrinsically straining vdW heterojunctions in-situ, without the need to apply external mechanical strain.

The vdW piezoelectric α-In_2Se_3 crystallizes in the *R*3*m* structure,[21] and has an IP lattice constant *a* of 4.026 Å.[22] The piezoelectricity consists of domains with both IP and OOP polarizations at room temperature. Notably, such piezoelectric polarization is retained down to the monolayer.[23] The hysteretic conductance resulting from the electric polarization in α-In_2Se_3 has been utilized to create ferroelectric field-effect transistors with a large on-off ratio, for which the α-In_2Se_3 layer simultaneously acts as the gate-oxide and channel material.[24] In an earlier study of Fe_3GeTe_2 on α-In_2Se_3[10] the reduction of the coercivity of Fe_3GeTe_2 was observed in magneto-optical Kerr effect experiments. A bias voltage had to be continuously applied, which was ascribed to the presence of an interfacial polymer layer. The multifunctional properties of α-In_2Se_3 make it a strong candidate material for in-memory computing applications that overcome the von Neumann bottleneck.[25] These properties of α-In_2Se_3 may also be useful in functionalizing other atomically thin vdW materials, including 2D magnets, by inducing an interfacial Dzyaloshinskii–Moriya interaction that can result in the emergence of magnetic skyrmions.[26]

In this work, we report the strain-induced modification of magnetic properties at a heterojunction between α-In_2Se_3 and the prototypical vdW ferromagnet Fe_3GeTe_2. An increased domain wall density and reductions in T_C point to a decrease in the exchange stiffness *A*. Density functional theory (DFT) calculations and atomistic spin dynamics simulations show that for Fe_3GeTe_2, a compressive strain of 0.4% is consistent with a reduction of exchange stiffness *A* and uniaxial anisotropy K_u, corresponding to a decrease of 20 K in T_C. Enhancement of H_c suggests strain-induced magnetostriction to affect the ferromagnetic hysteresis within the heterojunction. Modifications in the lattice structure at atomic length scales are further corroborated by comparison to a graphite/α-In_2Se_3 heterostructure. Specifically, a reduction in the Tuinstra-Koenig relation, $I(D)/I(G)$, in which $I(D)$ and $I(G)$ are the respective Raman peak intensities, is observed. For the Fe_3GeTe_2/α-In_2Se_3 heterojunction, magnetostrictive domain patterns with preferential orientations show ferromagnetism which is modulated by the polarization of the piezoelectric domains. These findings demonstrate that the incorporation of α-In_2Se_3 in vdW heterostructures may provide a general approach to electrostatically strain vdW interfaces within the confines of an atomically flat environment afforded by hBN encapsulation, thereby enabling the further study of the intrinsic properties of 2D magnets, graphene-based moiré systems and other air-sensitive transition-metal dichalcogenides (TMDs) and halides as a function of strain.

2. Results and Discussion

Fe_3GeTe_2 is a prototypical vdW magnet with a relatively high bulk T_C of 220 K which is stabilized by a large perpendicular magnetic anisotropy (PMA).[3] In bulk Fe_3GeTe_2, meander-style domains form as a result of the PMA and dipolar interaction.[3] In the atomically thin limit, monodomains become energetically favorable due to the large PMA. This work utilizes a Fe_3GeTe_2 flake of thickness 9 nm (Figure S3, Supporting Information), which is characterized by the meander domains described above (**Figure 1**).

At the Fe_3GeTe_2/α-In_2Se_3 heterojunction, the size of the magnetic domains decreases, and the domain wall density increases (Figure 1). As a first approximation, this size change commonly indicates a change in the stray field energy, which is proportional to J_S^2, in which J_S is the saturation magnetization.[27] Among the Fe_xGeTe_2 (x = 3, 4, 5) class of high-T_C itinerant vdW magnets, the saturation magnetization varies from 1.4[28] to 1.9 μ_B/Fe.[29] A large increase in J_S should result in a larger magnetic contrast within the heterojunction, i.e., a larger X-ray magnetic circular dichroism (XMCD) signal. However, there is no discernible difference between the amplitude of line profiles of the XMCD from the Fe_3GeTe_2/α-In_2Se_3 heterojunction and from the Fe_3GeTe_2 homojunction in Figure 1, revealing that J_S for this large-PMA material is likely homogeneous (Figure S5, Supporting Information). This may be due to the low measurement temperature of 50 K, which is significantly below T_C,[3] resulting in a non-varying magnetization *m*. The fact that there is no difference in XMCD between the Fe_3GeTe_2 homojunction and the Fe_3GeTe_2/α-In_2Se_3 heterojunction demonstrates that if there is a change in J_S at the heterojunction at 50 K, it has to be below the detection threshold of X-ray photoemission electron microscopy (XPEEM).

Alternatively, the change in size of the magnetic domains can also originate from a reduction in *A*. For uniaxial materials, the

E. Heppell, D. Backes, F. Maccherozzi, G. van der Laan
Diamond Light Source
Harwell Science and Innovation Campus
Didcot OX11 0DE, UK

E. Heppell
STFC/ISIS
Rutherford Appleton Laboratory
Didcot OX11 0QX, UK

K. Watanabe
Research Center for Electronic and Optical Materials
National Institute for Materials Science
1-1 Namiki, Tsukuba 305-0044, Japan

T. Taniguchi
Research Center for Materials Nanoarchitectonics
National Institute for Materials Science
1-1 Namiki, Tsukuba 305-0044, Japan

D. A. Mayoh, G. Balakrishnan
Department of Physics
University of Warwick
Coventry CV4 7AL, UK

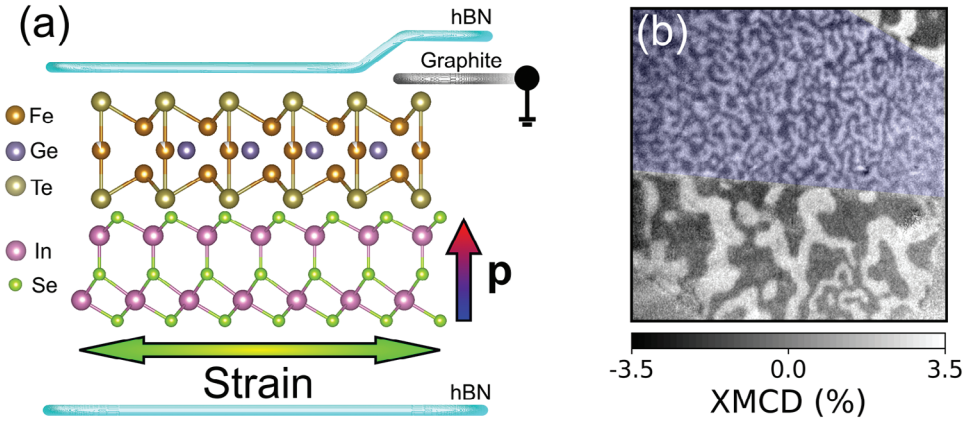

Figure 1. Interfacial coupling between the vdW ferromagnet Fe_3GeTe_2 and vdW piezoelectric α-In_2Se_3. a) Cross-sectional schematic of the hBN-encapsulated heterojunction showing strain and electric polarization **p** in the α-In_2Se_3 layer. A graphite electrode provides a conductive pathway between the sample and XPEEM sample holder. b) XPEEM image of the Fe_3GeTe_2 homojunction and the Fe_3GeTe_2/α-In_2Se_3 heterojunction obtained at 50 K (shaded in pale blue). Field of view = 15 µm.

domain wall energy, γ, is proportional to $\sqrt{AK_u}$.[27] For reduced A, it is energetically less costly to form domain walls within the Fe_3GeTe_2/α-In_2Se_3 heterojunction, resulting in an increase in the number of domains per unit area. The lack of any intermediate contrast in Figure 1 demonstrates that the heterojunction retains a large K_u comparable to A, although a slight reduction in K_u has been found in Fe_5GeTe_2, and can therefore not be completely ruled out.[30] Therefore, the change in the ferromagnetic domain structure could be due to a reduction of the magnetic anisotropy energy, which has been realized in strain-tuned[9] and ionically gated Fe_3GeTe_2.[31]

For reduced exchange stiffness A, a reduction in T_C, which is proportional to A,[27] should also occur. **Figure 2** shows the XMCD of the homojunction and heterojunction at

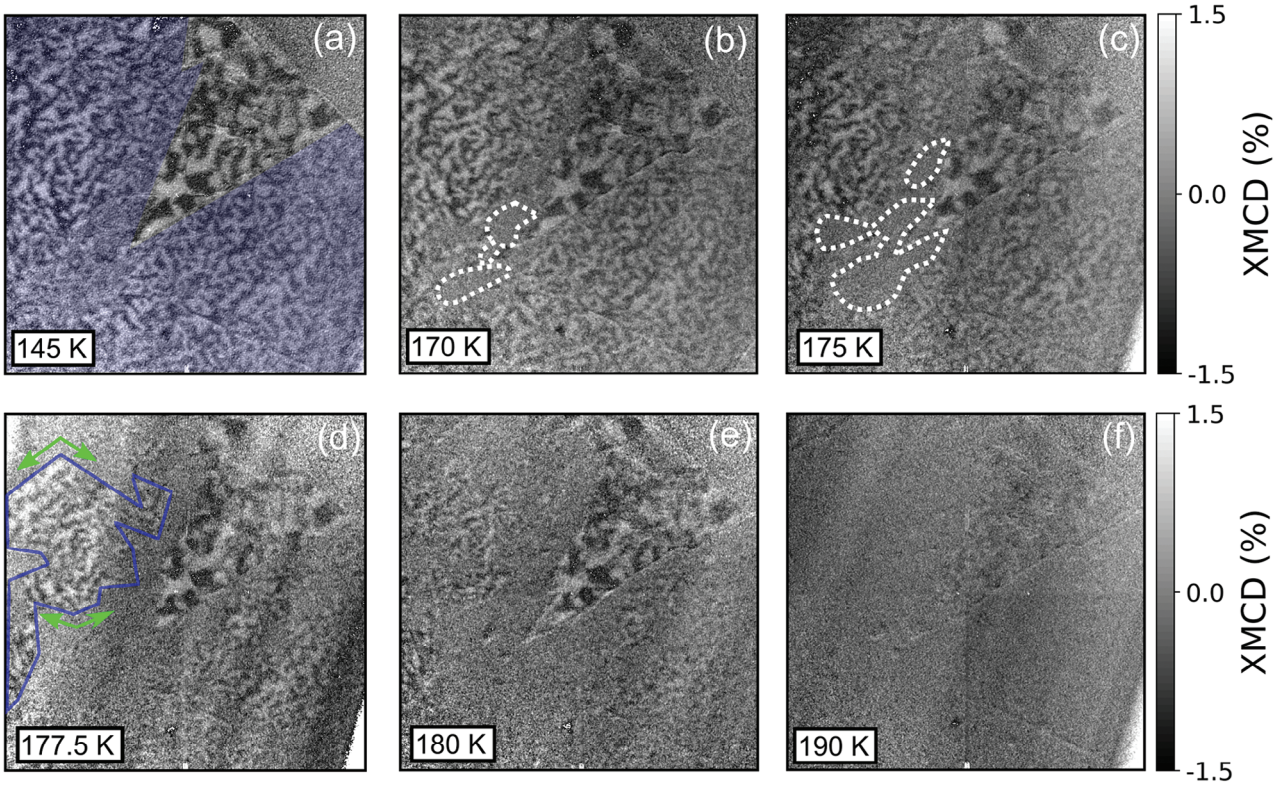

Figure 2. Reduction of the ferromagnetic T_C in a Fe_3GeTe_2/α-In_2Se_3 heterojunction (shaded in pale blue). XPEEM images of ferromagnetic domains in the Fe_3GeTe_2 homojunction and the Fe_3GeTe_2/α-In_2Se_3 heterojunction collected at a) 145 K, b) 170 K, c) 175 K, d) 177.5 K, e) 180 K, and f) 190 K. At 177.5 K, the magnetic contrast (encircled by the blue line) is modulated by geometric features shown by the green arrows. Field of view = 15 µm.

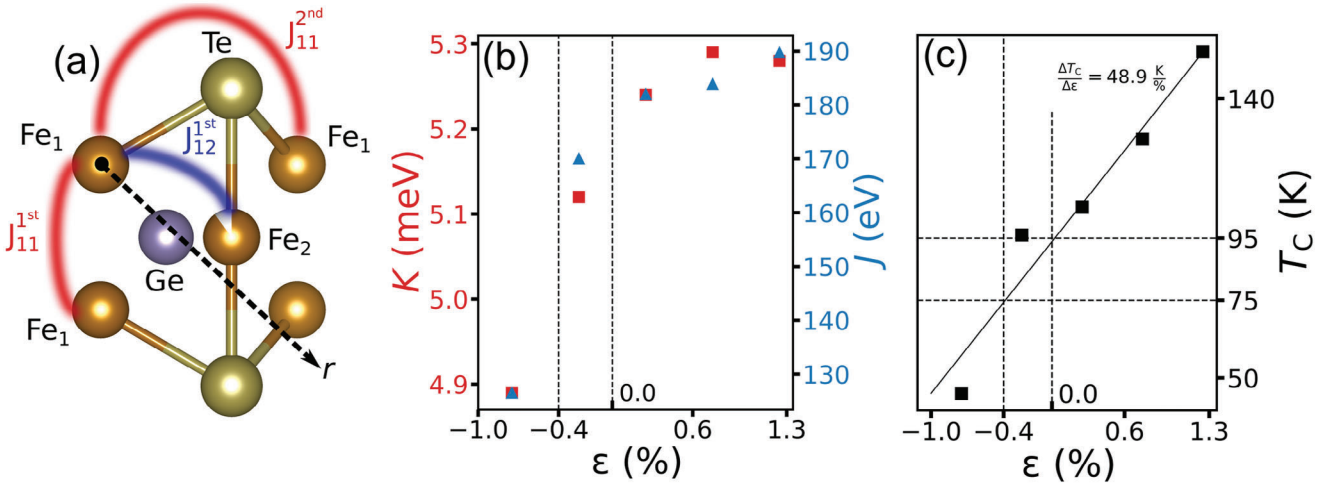

Figure 3. DFT calculations of K and J and estimated T_C for varying strain ϵ. a) Illustration of Fe_1 and Fe_2 sites and the respective exchange interactions J_{11} and J_{12} for monolayer Fe_3GeTe_2. Exchange interactions among nearest neighbors are considered for $r = 4.80$ Å. b) The uniaxial anisotropy constant K and the effective exchange coupling at the Fe_1 site, $J = \sum_a Z_a J_{ij}^a$,[34] are shown for varying strain ϵ. c) T_C as a function of varying strain ϵ. A linear fit of the data show that for a decrease of 20 K in T_C, from 95 to 75 K, the unit cell is compressively strained by ε = −0.4%.

temperatures ranging from 145 and 190 K. At 145 K, magnetic domains are present in both the homojunction and the heterojunction, while at 170 K, a small area within the heterojunction (encircled by the white dashed line) appears to be no longer magnetic (Figure 2b). This non-magnetic region expands to a larger area at 175 K (Figure 2c). At 177.5 K, the magnetic contrast is further reduced within the heterojunction (Figure 2d). At 190 K, the magnetic contrast within the homojunction is barely visible (Figure 2f), meaning that the T_C decreases by up to ≈20 K.

Notably, at 177.5 K (Figure 2d), the area encircled by the blue line, which lies within the heterojunction, remains magnetic and has geometric features resembling a threefold symmetry reminiscent of the $R3m$ space group of α-In_2Se_3.[23] Presumably, the T_C of the Fe_3GeTe_2 within the heterojunction is affected by the varying polarizations of the piezoelectric domains of the underlying α-In_2Se_3.

The effective exchange coupling (J) and K_u of monolayer Fe_3GeTe_2 are calculated using density functional theory (DFT). Using these parameters in atomistic spin dynamics, Curie temperatures are estimated for monolayer Fe_3GeTe_2 with varying lattice constant a (**Figure 3**). Specifically, a decrease of 20 K in T_C corresponds to a compressive strain ϵ = −0.4% relative to the IP lattice parameter $a_0 = 4.01$ Å.[32] This is consistent with pressure-induced compression of powdered Fe_3GeTe_2, for which a compressive strain ε = −0.5%. induces a similar change in T_C of ≈20 K.[33]

The coupling between α-In_2Se_3 and Fe_3GeTe_2 also enhances H_c. Field-induced domain reversal is observed only for the homojunction. Upon application of a field pulse H_{OOP} = +88 mT, the heterojunction retains its initial saturation magnetization, which was formed by cooling the sample in a field H_{OOP} = −13.2 mT across T_C (**Figure 4**). As a first approximation, consideration of the Stoner-Wohlfarth model,[35] in which H_c is proportional to K_u, suggests an increase in the uniaxial anisotropy within the heterojunction.[9,36] However, an enhanced K_u contradicts the large density of domain walls in the virgin state (Figures 1 and 2), with energy $\gamma \propto \sqrt{AK_u}$, for which an enhancement of K_u is energetically costly within the heterojunction. Furthermore, an enhanced uniaxial anisotropy would also likely enhance T_C in this material,[31] which is contrary to the results presented in Figure 2. In other words, the enhancement of H_c within the heterojunction is unlikely to originate from increased K_u, and is likely to be at least partially governed by extrinsic mechanisms, including strain-induced domain wall pinning[37] or magnetostriction effects.[36]

Strain within the Fe_3GeTe_2/α-In_2Se_3 heterojunction is characterized by comparison to Raman spectroscopy measurements of an α-In_2Se_3/graphite reference heterostructure. In particular, the Tuinstra-Koenig ratio, $1/L_a \propto I(D)/I(G)$, where $I(D)$ and $I(G)$ are the intensities of the respective D and G Raman peaks and L_a is the crystallite size, is a measure of the amount of disorder.[38] Such disorder can originate from point-like defects, including vacancies induced by ion bombardment[39,40] and dislocations,[41] or grain boundaries in nanocrystalline graphite.[38] The chances of a chalcogen occupying a vacancy in the graphite lattice and contributing to Raman scattering are extremely unlikely due to negligible vdW diffusion. Therefore, we consider the role of dislocations and the grain boundaries of graphene crystallites, rather than vacancies.

In detail, the Raman spectra of the graphite (Figure S6, Supporting Information) include the 2D, G, and D peaks, indicating the presence of finite disorder. The lack of a D' peak, peak attenuation, or broadening[40] indicate that the degree of disorder is somewhere in between that of graphite and nanocrystalline graphite, for which the Tuinstra-Koenig ratio is valid.[42] **Figure 5**a shows a reduction in $I(D)/I(G)$ within the graphite/α-In_2Se_3 interface. As mentioned above, the disorder is likely due to dislocations or grain boundaries between crystallites, rather than vacancies, suggesting the migration of dislocations[41] or grain boundaries[43,44] in response to a compressive strain induced by the α-In_2Se_3 at the interface. There also seems to

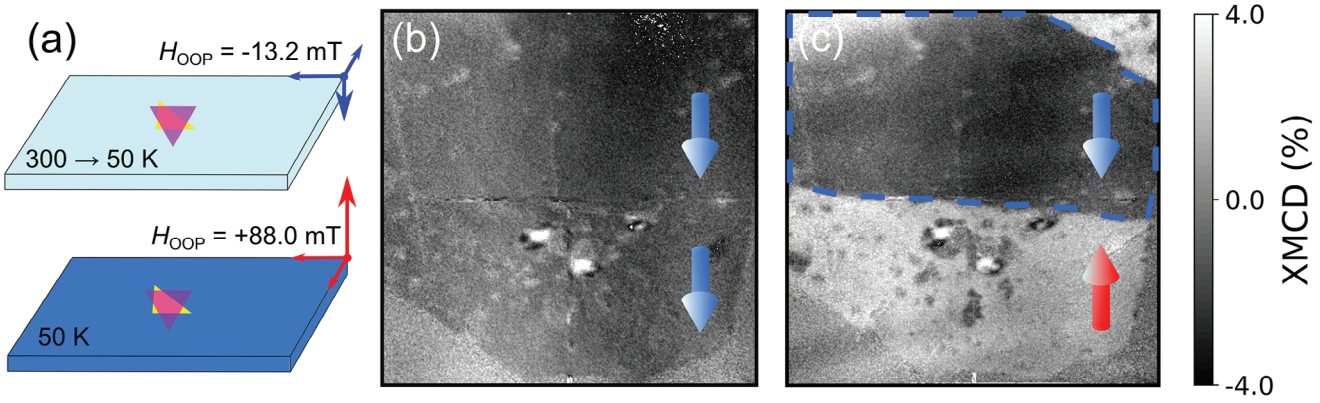

Figure 4. Enhanced magnetic coercivity H_c of the Fe_3GeTe_2/α-In_2Se_3 heterojunction at 50 K. a) The magnetic state is initialized by field-cooling the sample from 300 to 50 K in a field $H_{OOP} = -13.2$ mT. At 50 K, a field $H_{OOP} = +88$ mT of opposite polarity is applied, resulting in a partially field-reversed state. XPEEM images of the initial state and partially field-reversed state are shown in b, c), respectively. The magnetization directions (up, down) are depicted by the (red, blue) arrows. The Fe_3GeTe_2 homojunction and the Fe_3GeTe_2/α-In_2Se_3 heterojunction are demarcated by the blue dashed line. Field of view = 15 µm.

be a marginal enhancement of $I(D)/I(G)$ at the tip of the α-In_2Se_3 flake (Figure 5a). The AFM measurement (Figure S8b, Supporting Information) shows variations of the α-In_2Se_3 thickness, which may result in piezoelectric domains with varying polarization. We note that there are no frequency shifts or peak splittings of the G or $2D$ modes (Figure S6, Supporting Information), which have been observed for mechanically strained graphene films on flexible substrates.[45,46] We attribute this to sample-dependent piezoelectric polarization of α-In_2Se_3 and superlubricity of incommensurately stacked graphene.[47,48]

Raman measurements of a separate Fe_3GeTe_2/α-In_2Se_3 heterojunction sample show a blueshift of the E_g^2 mode by $\omega_1 = 3.5$ cm^{-1} and a redshift of the A_g^1 mode by $\omega_2 = 9.2$ cm^{-1} (Figure 5d; Table S1, Supporting Information).[49] The A_g^1 and E_g^2 modes shift in opposite directions, respectively, compared to the Raman shifts observed in Fe_3GeTe_2 subject to compressive pressure,[33] indicating a tensile strain within this sample. Direct comparison to Raman spectroscopy measurements of strained MoS_2[50] and WS_2[51] implies a remarkably large tensile strain of 2–3% (Table S2, Supporting Information). We leave the characterization of interfacial strain within TMD/α-In_2Se_3 heterointerfaces as a topic of future study. Rashba-type spin-orbit splitting has been observed at vdW interfaces with high carrier mobilities,[52,53] and could also be envisioned to affect the ferromagnetic domain structure at the Fe_3GeTe_2/α-In_2Se_3 interface.[2,54]

It is necessary to consider the characteristic length of the piezoelectric domains in α-In_2Se_3. Piezoresponse force microscopy (PFM) imaging of α-In_2Se_3 show piezoelectric domains which are 5–15 µm in length (Figure 5b). These share a common length scale with the geometric features modulating the ferromagnetic domain structure at 177.5 K (Figure 2b), which are also on the order of several µm, while the piezoelectric domain walls in α-In_2Se_3 are much too narrow[55] to account for the size of the magnetic modulations.

In general, strain can induce magnetostriction in ferromagnets. When coupled to the piezoelectric α-In_2Se_3, the magnetic domains in Fe_3GeTe_2 (Figure 5c) have preferential orientations (Figure 5d), which manifest due to the preferential domain alignment stemming from the $R3m$ space group of α-In_2Se_3. For a material with large PMA and significant magnetostriction constant,[56] the preferential alignment of OOP domains in response to an IP strain as seen in Figure 5c may be due to a small IP magnetization induced by the stress anisotropy.

The preferential alignment of piezoelectric domains in α-In_2Se_3 is also visible in the PFM data. For the hypothetical case where the piezoelectric domains are fully polarized IP, the domain polarization should exhibit a three-fold symmetry consistent with the $R3m$ space group. The OOP PFM phase shift response shown in Figure 5b is only ≈40° (Figure S11, Supporting Information), opposed to a 180° phase shift found for oppositely polarized domains, suggesting the simultaneous existence of IP and OOP components,[23,57,58] meaning that the preferential alignment of piezoelectric (Figure 5b) and ferromagnetic (Figure 5c) domains originate from a finite IP piezoelectric component. Contrarily, the OOP piezoelectric component observed in α-In_2Se_3 would likely have a negligible effect on the ferromagnetic domains in Fe_3GeTe_2, especially in the case of the 2H phase of α-In_2Se_3, for which an even-odd thickness dependence of the d_{33} piezoelectric component has been reported.[59]

Such magnetostriction of domains is well-documented for crystalline ferromagnets, for which the magnetic domain walls are commensurate with grain boundaries between neighboring stress states.[60–62] The magnetostriction observed in the present case (Figure 5c) is distinct from that observed in crystalline ferromagnets, for which the induced stress anisotropy $K_s = 3/2\,\lambda_s\sigma$, where λ_s is the magnetostriction constant and σ is the applied stress,[27] is on the order of the magnetocrystalline anisotropy.[60,63] Here, K_s is much weaker than the intrinsically strong uniaxial anisotropy K_u of Fe_3GeTe_2, as no full OOP-to-IP spin reorientation transition is observed.

Nevertheless, a small IP magnetization component might be present within the heterojunction. By obtaining the XMCD signal for 0° and 90° azimuths, IP component of the magnetization can be derived.[30] In detail, for domains that are fully magnetized OOP, the XMCD with respect to azimuthal angle is constant, while for domains which are magnetized IP, the XMCD should sinusoidally vary with the azimuthal angle. We observe a pronounced azimuthal dependence of the XMCD within the

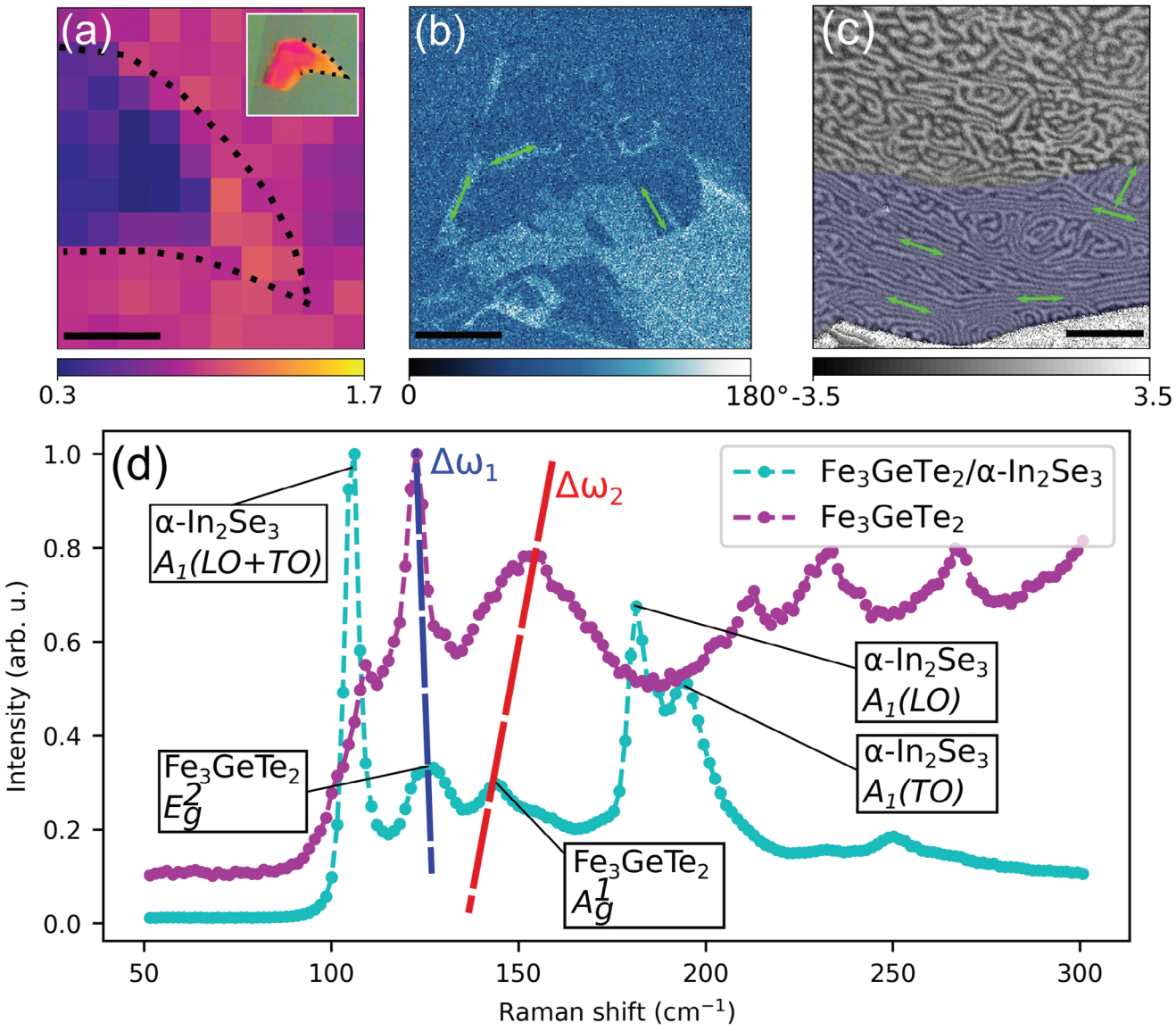

Figure 5. Interfacial strain within α-In_2Se_3 heterojunctions. a) Plot of $I(D)/I(G)$ of a graphite/α-In_2Se_3 heterostructure obtained at 300 K. There is a significant reduction of $I(D)/I(G)$ for the left part of the α-In_2Se_3 flake, while a slight enhancement of $I(D)/I(G)$ is visible at the tip. The inset shows an optical micrograph with the α-In_2Se_3 flake is indicated by the dashed black line. Scale bar = 5 µm. b) PFM phase response of a α-In_2Se_3 flake taken at 300 K. The thickness of the α-In_2Se_3 flake varies between 60 and 140 nm. Preferential directions of piezoelectric domains are indicated by green arrows. Scale bar = 5 µm. c) XPEEM image of magnetostrictive domains (indicated by green arrows) in Fe_3GeTe_2/α-In_2Se_3 taken at 100 K. The heterojunction in shaded in pale blue. Field of view = 17.5 µm and scale bar = 5 µm. d) Raman spectra of a Fe_3GeTe_2 homojunction and a Fe_3GeTe_2/α-In_2Se_3 heterojunction. The Fe_3GeTe_2 A_g^1 mode blueshifts by $\Delta\omega_1 = +3.5$ cm^{-1} and the combined $A_g^1 + E_g^2$ mode redshifts by $\Delta\omega_2 = -9.2$ cm^{-1}.

heterojunction (Figure S13, Supporting Information). However, the small domain width and the presence of astigmatism in the XMCD images obfuscates a definitive conclusion regarding the presence of IP magnetization.

Compared to epitaxially grown heterostructures[16] and crystalline thin films,[63] the limited IP magnetization component may reflect the intrinsically weak mechanical coupling at the vdW heterojunction. Nevertheless, the previously derived compressive strain of 0.4% can still result in a coefficient $K_s = 0.38$ meV/Fe atom along the stress axis (see Supporting Information), where $\lambda_s = -559 \times 10^{-6}$.[56] This is less, but within the same order of magnitude as $K_u = 0.844$ meV/Fe atom, and is large enough to cause a decrease in the total magnetic anisotropy energy for compressive strains.[56] A magnetostriction-induced deviation of the easy axis of Fe_3GeTe_2 would align magnetic domains along lower-anisotropy directions, and would also increase H_c, as previously demonstrated in Figure 4b.

3. Conclusion

The strain-tuning of magnetic properties, including T_C, the magnetic anisotropy, and the exchange parameters, can enable the

formation of emergent magnetic ground states in atomically thin magnets. We demonstrate strain-induced modulation of ferromagnetism at a vdW heterojunction consisting of Fe_3GeTe_2 and α-In_2Se_3 within the confines of an atomically smooth environment provided by encapsulation between thin layers of hBN. In summary, we observe a decrease in T_C of about 20 K corresponding to a compressive strain of 0.4%, and strain-induced magnetostriction which induces preferential alignment of magnetic domains and a larger coercive field H_c. We expect our results to enable the study of strain-dependent intrinsic properties of other 2D atomically abrupt heterostructures, including hBN-encapsulated TMDs and graphene-based moiré heterostructures.

4. Experimental Section

Bulk Crystal Growth and Characterization: Fe_3GeTe_2 and α-In_2Se_3 crystals were grown by the chemical vapor transport technique using iodine as the transport agent, yielding single crystalline hexagonal platelets of approximately 3×3 mm^2 in case of Fe_3GeTe_2[32] and 2×2 mm^2 sized hexagonal silvery-blue platelets in case of α-In_2Se_3.[22] The crystals were characterized by x-ray diffraction (XRD) using a Panalytical X-Pert Pro MPD Kα1 and by energy-dispersive x-ray spectroscopy (EDX) using a Zeiss SUPRA 55-VP FEGSEM.

X-ray diffraction patterns were obtained on single crystals mounted with the *ab* plane parallel to the x-ray beam. When the scattering angle was zero, only the (00*l*) reflections should be observed in this geometry. Figure S1 (Supporting Information) shows the diffraction pattern obtained exhibiting reflections typical of the α-In_2Se_3 structure. Compositional analysis of the crystals obtained was carried out using EDX analysis. The composition of the single crystals was estimated to be $In_{1.96(5)}Se_{3.04(5)}$.

Mechanical Exfoliation: Bulk α-In_2Se_3, Fe_3GeTe_2, graphite and hexagonal boron nitride (hBN) crystals were mechanically exfoliated in an inert Ar-filled glovebox with O_2 and H_2O concentrations below 1 ppm. Thin flakes were identified by optical microscopy, and were stacked layer-by-layer with a polydimethylsiloxane (PDMS)-assisted transfer over a conductive Au-coated silicon oxide substrate (Figure S2, Supporting Information).

Magnetic Domain Imaging with XPEEM: X-ray photoemission electron microscopy (XPEEM) measurements were conducted at the UE49/PGMa beamlime at BESSY II (Helmholtz-Zentrum Berlin)[64] and at beamline I06 at Diamond Light Source. Real-space X-ray absorption (XAS) and X-ray magnetic circular dichroism (XMCD) measurements at the Fe L_3 edge (706.2 eV) were performed from 50-200 K. The fixed angle of incidence of the incoming X-rays with respect to the sample surface was 16°, which means that 28% of the sample's out-of-plane magnetization component was projected along the X-ray propagation direction.[65] The XMCD asymmetry was defined as $(\sigma_- - \sigma_+)/(\sigma_- + \sigma_+)$, where σ_- and σ_+ are the XAS signals at the maximum taken with left and right circularly polarized X-rays, respectively.

Raman Microscopy of Fe_3GeTe_2, α-In_2Se_3, and Graphite: hBN-encapsulated Fe_3GeTe_2, α-In_2Se_3, and graphite flakes were characterized with Raman spectroscopy at room temperature. The data were collected using an objective lens with 100x magnification. The laser wavelength was λ = 473 nm. The laser power was limited to 3.5 mW to limit laser-induced damage of the sample. The accumulation time was 120 s.

Characterization of Piezoelectricity in α-In_2Se_3 with PFM: Instrumentation and Setup: Single frequency vertical piezoresponse force microscopy (PFM) measurements were performed on an exfoliated α-In_2Se_3 (75-125 nm)/hBN (10 nm) flake placed on p-Si/h-N (17 nm) substrate using a scanning probe microscope within a variable temperature cryostat (Attocube systems). The employed Pt-Ir conductive tip (Nanosensors) had a radius of curvature <25 nm, spring constant of ≈3.6 Nm^{-1}, and resonance frequency of 67.2 kHz. PFM measurements were performed at temperatures of 50 and 294 K with a stability of <20 mK.

Characterization of Piezoelectricity in α-In_2Se_3 with PFM: Measurement Procedures: First, the flake of interest was located via contact mode AFM imaging. Next, an ac drive voltage of V_{pp} = 10 V was applied to the tip while in contact with the sample surface to excite piezoresponse at an off-resonance frequency of 80 kHz (contact resonance ≈335 kHz). Off-resonance PFM was used to minimize topography cross-talk.[66–68] The amplitude and phase-shift of the tip-sample excitation, corresponding to the PFM signal, were detected using a lock-in amplifier. PFM images were acquired at each imaging temperature over a 20 µm region with 256 sampling points.

DFT Calculations of K_U, J, T_C and Lattice Parameter a: First-principles density functional theory (DFT) calculations with fully relativistic PAW pseudopotentials were performed with Quantum ESPRESSO.[69] The exchange and correlation effects were treated within the local density approximation (LDA).[70] LDA+U calculations overestimate the magnetic moments of Fe,[56] as shown in Section S13 (Supporting Information). The DFT calculations were carried out without considering U parameters. The plane-wave cut-off energy of 70 Ry and a $18 \times 18 \times 1$ k-point mesh in the irreducible Brillouin zone were used in the calculations. Spin-orbit coupling was included in all electronic structure calculations.

The tight-binding Hamiltonians were constructed using Wannier90[71] and then, TB2J[72] was used to calculate the exchange parameters considering nearest neighbors within 4.80 Å. Anisotropic exchange parameters were also considered, as implemented in TB2J for spin-orbit coupling interactions.

The Curie temperature was calculated by using atomistic spin dynamics as implemented in Vampire with Monte Carlo simulations.[73]

Supporting Information

Supporting Information is available from the Wiley Online Library or from the author.

Acknowledgements

R.F. and T.H. acknowledged financial support from the Oxford-ShanghaiTech collaboration project and the Engineering and Physical Sciences Research Council (projects EP/N032128/1 and EP/X015793/1). The authors thank the Helmholt-Zentrum Berlin für Materialien und Energie for allocation of synchrotron radiation beamtime on beamline UE49 at the BESSY II electron storage ring (212-10475-ST), and Diamond Light Source for provision of beamtime at beamline I06 (MM31730). A.K.J.T., A.S. and P.H. acknowledged the SpOT-LITE program (Grant No. A18A6b0057) and AlScN ferroelectrics program (Grant No. A20G9b0135), both funded by Singapore's RIE2020 initiatives. K.W. and T.T. acknowledged support from the JSPS KAKENHI (Grant Numbers 21H05233 and 23H02052) and World Premier International Research Center Initiative (WPI), MEXT, Japan. M.A.M. acknowledged financial support from the Deutsche Forschungsgemeinschaft (Project No. 328545488; TRR 227, Project A03). R.F. thanks Dr. Matthew Watson (I05), Dr. Tina Geraki (I18), and Dr. Sahil Tippireddy (Materials Characterization Lab) for allowing respective access to the glovebox, Raman spectrometer, and AFM at the Diamond Light Source.

Conflict of Interest

The authors declare no conflict of interest.

Author Contributions

R.F., G.v.d.L., and T.H. conceived the experiment. R.F. synthesized the exfoliated samples. R.F., M.A.M., Ale.S. and F.K. performed XPEEM measurements at BESSY. A.K.J.T., A.S., and P.H. performed PFM measurements. R.F., A.S., E.H., D.B. and F.M. performed XPEEM measurements at the Diamond Light Source. R.F. performed Raman spectroscopy measurements.

K.W. and T.T. grew bulk hBN crystals. D.M. and G.B. grew bulk Fe_3GeTe_2 and α-In_2Se_3 crystals. R.F., G.v.d.L. and T.H. wrote the manuscript with input from all authors. All authors discussed the results and reviewed the paper. The data that support the findings of this study are available from the corresponding author upon reasonable request.

Data Availability Statement

The data that support the findings of this study are available from the corresponding author upon reasonable request.

Keywords

2D materials, magnetic materials, piezoelectric materials, van der Waals materials

Received: January 22, 2024
Revised: February 27, 2024
Published online: March 14, 2024

[1] B. Huang, G. Clark, E. Navarro-Moratalla, D. R. Klein, R. Cheng, K. L. Seyler, D. Zhong, E. Schmidgall, M. A. McGuire, D. H. Cobden, W. Yao, D. Xiao, P. Jarillo-Herrero, X. Xu, *Nature* **2017**, *546*, 270.
[2] Y. Wu, S. Zhang, J. Zhang, W. Wang, Y. L. Zhu, J. Hu, G. Yin, K. Wong, C. Fang, C. Wan, X. Han, Q. Shao, T. Taniguchi, K. Watanabe, J. Zang, Z. Mao, X. Zhang, K. L. Wang, *Nat. Commun.* **2020**, *11*, 3.
[3] Z. Fei, B. Huang, P. Malinowski, W. Wang, T. Song, J. Sanchez, W. Yao, D. Xiao, X. Zhu, A. F. May, W. Wu, D. H. Cobden, J.-H. Chu, X. Xu, *Nat. Mater.* **2018**, *17*, 778.
[4] B. Huang, J. Cenker, X. Zhang, E. L. Ray, T. Song, T. Taniguchi, K. Watanabe, M. A. McGuire, D. Xiao, X. Xu, *Nat. Nano.* **2020**, *15*, 212.
[5] D. Zhong, K. L. Seyler, X. Linpeng, R. Cheng, N. Sivadas, B. Huang, E. Schmidgall, T. Taniguchi, K. Watanabe, M. A. McGuire, W. Yao, D. Xiao, K.-M. C. Fu, X. Xu, *Sci. Adv.* **2017**, *3*, e1603113.
[6] D. R. Klein, D. MacNeill, Q. Song, D. T. Larson, S. Fang, M. Xu, R. A. Ribeiro, P. C. Canfield, E. Kaxiras, R. Comin, P. Jarillo-Herrero, *Nat. Phys.* **2019**, *15*, 1255.
[7] C. Xu, J. Feng, M. Kawamura, Y. Yamaji, Y. Nahas, S. Prokhorenko, Y. Qi, H. Xiang, L. Bellaiche, *Phys. Rev. Lett.* **2020**, *124*, 087205.
[8] X. Zhang, L. Wang, H. Su, X. Xia, C. Liu, B. Lyu, J. Lin, M. Huang, Y. Cheng, J.-W. Mei, J.-F. Dai, *Nano Lett.* **2022**, *22*, 9891.
[9] Y. Wang, C. Wang, S.-J. Liang, Z. Ma, K. Xu, X. Liu, L. Zhang, A. S. Admasu, S.-W. Cheong, L. Wang, M. Chen, Z. Liu, B. Cheng, W. Ji, F. Miao, *Adv. Mater.* **2020**, *32*, 2004533.
[10] J. Eom, I. H. Lee, J. Y. Kee, M. Cho, J. Seo, H. Suh, H.-J. Choi, Y. Sim, S. Chen, H. J. Chang, S.-H. Baek, C. Petrovic, H. Ryu, C. Jang, Y. D. Kim, C.-H. Yang, M.-J. Seong, J. H. Lee, S. Y. Park, J. W. Choi, *Nat. Commun.* **2023**, *14*, 5605.
[11] K. S. Novoselov, A. Mishchenko, A. Carvalho, A. H. Castro Neto, *Science* **2016**, *353*, aac9439.
[12] D. Zhong, K. L. Seyler, X. Linpeng, N. P. Wilson, T. Taniguchi, K. Watanabe, M. A. McGuire, K.-M. C. Fu, D. Xiao, W. Yao, X. Xu, *Nat. Nano.* **2020**, *15*, 187.
[13] H. Wang, Y. Liu, P. Wu, W. Hou, Y. Jiang, X. Li, C. Pandey, D. Chen, Q. Yang, H. Wang, D. Wei, N. Lei, W. Kang, L. Wen, T. Nie, W. Zhao, K. L. Wang, *ACS Nano* **2020**, *14*, 10045.
[14] Y. Cao, V. Fatemi, S. Fang, K. Watanabe, T. Taniguchi, E. Kaxiras, P. Jarillo-Herrero, *Nature* **2018**, *556*, 43.
[15] D. J. Rizzo, B. S. Jessen, Z. Sun, F. L. Ruta, J. Zhang, J.-Q. Yan, L. Xian, A. S. McLeod, M. E. Berkowitz, K. Watanabe, T. Taniguchi, S. E. Nagler, D. G. Mandrus, A. Rubio, M. M. Fogler, A. J. Millis, J. C. Hone, C. R. Dean, D. N. Basov, *Nano Lett.* **2020**, *20*, 8438.
[16] M.-Y. Li, Y. Shi, C.-C. Cheng, L.-S. Lu, Y.-C. Lin, H.-L. Tang, M.-L. Tsai, C.-W. Chu, K.-H. Wei, J.-H. He, W.-H. Chang, K. Suenaga, L.-J. Li, *Science* **2015**, *349*, 524.
[17] F. Pizzocchero, L. Gammelgaard, B. S. Jessen, J. M. Caridad, L. Wang, J. Hone, P. Boggild, T. J. Booth, *Nat. Commun.* **2016**, *7*, 11894.
[18] F. He, Y. Zhou, Z. Ye, S.-H. Cho, J. Jeong, X. Meng, Y. Wang, *ACS Nano* **2021**, *15*, 5944.
[19] N. P. Kazmierczak, M. Van Winkle, C. Ophus, K. C. Bustillo, S. Carr, H. G. Brown, J. Ciston, T. Taniguchi, K. Watanabe, D. K. Bediako, *Nat. Mater.* **2021**, *20*, 956.
[20] W.-M. Zhao, L. Zhu, Z. Nie, Q.-Y. Li, Q.-W. Wang, L.-G. Dou, J.-G. Hu, L. Xian, S. Meng, S.-C. Li, *Nat. Mater.* **2022**, *21*, 284.
[21] Y. Zhou, D. Wu, Y. Zhu, Y. Cho, Q. He, X. Yang, K. Herrera, Z. Chu, Y. Han, M. C. Downer, H. Peng, K. Lai, *Nano Lett.* **2017**, *17*, 5508.
[22] M. Küpers, P. M. Konze, A. Meledin, J. Mayer, U. Englert, M. Wuttig, R. Dronskowski, *Inorg. Chem.* **2018**, *57*, 11775.
[23] F. Xue, J. Zhang, W. Hu, W.-T. Hsu, A. Han, S.-F. Leung, J.-K. Huang, Y. Wan, S. Liu, J. Zhang, J.-H. He, W.-H. Chang, Z. L. Wang, X. Zhang, L.-J. Li, *ACS Nano* **2018**, *12*, 4976.
[24] M. Si, A. K. Saha, S. Gao, G. Qiu, J. Qin, Y. Duan, J. Jian, C. Niu, H. Wang, W. Wu, S. K. Gupta, P. D. Ye, *Nat. Electron.* **2019**, *2*, 580.
[25] D. Ielmini, H.-S. P. Wong, *Nat. Electron.* **2018**, *1*, 333.
[26] K. Huang, D.-F. Shao, E. Y. Tsymbal, *Nano Lett.* **2022**, *22*, 3349.
[27] A. Hubert, R. Schäfer, *Magnetic Domains: The Analysis of Magnetic Microstructures*, 1st edition, Springer-Verlag, Berlin **1998**.
[28] S.-R. Kim, I. K. Park, J.-G. Yoo, J. Seo, J.-G. Kim, J.-H. Park, J. S. Kim, K. Kim, G. Lee, K.-T. Ko, *ACS Appl. Nano Mater.* **2022**, *5*, 10341.
[29] K. Yamagami, Y. Fujisawa, B. Driesen, C. H. Hsu, K. Kawaguchi, H. Tanaka, T. Kondo, Y. Zhang, H. Wadati, K. Araki, T. Takeda, Y. Takeda, T. Muro, F. C. Chuang, Y. Niimi, K. Kuroda, M. Kobayashi, Y. Okada, *Phys. Rev. B* **2021**, *103*, L060403.
[30] R. Fujita, P. Bassirian, Z. Li, Y. Guo, M. A. Mawass, F. Kronast, G. van der Laan, T. Hesjedal, *ACS Nano* **2022**, *16*, 10545.
[31] Y. Deng, Y. Yu, Y. Song, J. Zhang, N. Z. Wang, Z. Sun, Y. Yi, Y. Z. Wu, S. Wu, J. Zhu, J. Wang, X. H. Chen, Y. Zhang, *Nature* **2018**, *563*, 94.
[32] D. A. Mayoh, G. D. A. Wood, S. J. R. Holt, G. Beckett, E. J. L. Dekker, M. R. Lees, G. Balakrishnan, *Cryst. Growth Des.* **2021**, *21*, 6786.
[33] N.-T. Dang, D. P. Kozlenko, O. N. Lis, S. E. Kichanov, Y. V. Lukin, N. O. Golosova, B. N. Savenko, D.-L. Duong, T.-L. Phan, T.-A. Tran, M.-H. Phan, *Adv. Sci.* **2023**, *10*, 2206842.
[34] S. Jekal, *Condens. Matter.* **2019**, *4*, 11.
[35] E. C. Stoner, E. P. Wohlfarth, *Phil. Trans. Royal Soc. Ser. A* **1948**, *240*, 599.
[36] Y. Zhang, L. Shen, M. Liu, X. Li, X. Lu, L. Lu, C. Ma, C. You, A. Chen, C. Huang, L. Chen, M. Alexe, C.-L. Jia, *ACS Nano* **2017**, *11*, 8002.
[37] S. S. P. Parkin, M. Hayashi, L. Thomas, *Science* **2008**, *320*, 190.
[38] F. Tuinstra, J. L. Koenig, *J. Chem. Phys.* **2003**, *53*, 1126.
[39] M. M. Lucchese, F. Stavale, E. H. M. Ferreira, C. Vilani, M. V. O. Moutinho, R. B. Capaz, C. A. Achete, A. Jorio, *Carbon* **2010**, *48*, 1592.
[40] L. G. Cançado, A. Jorio, E. H. M. Ferreira, F. Stavale, C. A. Achete, R. B. Capaz, M. V. O. Moutinho, A. Lombardo, T. S. Kulmala, A. C. Ferrari, *Nano Lett.* **2011**, *11*, 3190.
[41] J. H. Warner, E. R. Margine, M. Mukai, A. W. Robertson, F. Giustino, A. I. Kirkland, *Science* **2012**, *337*, 209.
[42] A. C. Ferrari, D. M. Basko, *Nat. Nano.* **2013**, *8*, 235.
[43] V. K. Sangwan, D. Jariwala, I. S. Kim, K.-S. Chen, T. J. Marks, L. J. Lauhon, M. C. Hersam, *Nat. Nano.* **2015**, *10*, 403.
[44] S. Kurasch, J. Kotakoski, O. Lehtinen, V. Skákalová, J. Smet, C. E. I. Krill, A. V. Krasheninnikov, U. Kaiser, *Nano Lett.* **2012**, *12*, 3168.
[45] O. Frank, G. Tsoukleri, J. Parthenios, K. Papagelis, I. Riaz, R. Jalil, K. S. Novoselov, C. Galiotis, *ACS Nano* **2010**, *4*, 3131.
[46] Z. H. Ni, T. Yu, Y. H. Lu, Y. Y. Wang, Y. P. Feng, Z. X. Shen, *ACS Nano* **2008**, *2*, 2301.

[47] C. Androulidakis, E. N. Koukaras, G. Paterakis, G. Trakakis, C. Galiotis, *Nat. Commun.* **2020**, *11*, 1595.
[48] Y. Song, D. Mandelli, O. Hod, M. Urbakh, M. Ma, Q. Zheng, *Nat. Mater.* **2018**, *17*, 894.
[49] X. Kong, T. Berlijn, L. Liang, *Adv. Electron. Mater.* **2021**, *7*, 2001159.
[50] Z. Li, Y. Lv, L. Ren, J. Li, L. Kong, Y. Zeng, Q. Tao, R. Wu, H. Ma, B. Zhao, D. Wang, W. Dang, K. Chen, L. Liao, X. Duan, X. Duan, Y. Liu, *Nat. Commun.* **2020**, *11*, 1151.
[51] S. Pak, J. Lee, Y.-W. Lee, A.-R. Jang, S. Ahn, K. Y. Ma, Y. Cho, J. Hong, S. Lee, H. Y. Jeong, H. Im, H. S. Shin, S. M. Morris, S. Cha, J. I. Sohn, J. M. Kim, *Nano Lett.* **2017**, *17*, 5634.
[52] K. Premasiri, S. K. Radha, S. Sucharitakul, U. R. Kumar, R. Sankar, F.-C. Chou, Y.-T. Chen, X. P. A. Gao, *Nano Lett.* **2018**, *18*, 4403.
[53] T. S. Ghiasi, A. A. Kaverzin, P. J. Blah, B. J. van Wees, *Nano Lett.* **2019**, *19*, 5959.
[54] S. Albarakati, C. Tan, Z.-J. Chen, J. G. Partridge, G. Zheng, L. Farrar, E. L. H. Mayes, M. R. Field, C. Lee, Y. Wang, Y. Xiong, M. Tian, F. Xiang, A. R. Hamilton, O. A. Tretiakov, D. Culcer, Y.-J. Zhao, L. Wang, *Sci. Adv.* **2019**, *5*, eaaw0409.
[55] E. Han, S. M. Nahid, T. Rakib, G. Nolan, P. F. Ferrari, M. A. Hossain, A. Schleife, S. Nam, E. Ertekin, A. M. van der Zande, P. Y. Huang, *ACS Nano* **2023**, *17*, 7881.
[56] H. L. Zhuang, P. R. C. Kent, R. G. Hennig, *Phys. Rev. B.* **2016**, *93*, 134407.
[57] J. Xiao, H. Zhu, Y. Wang, W. Feng, Y. Hu, A. Dasgupta, Y. Han, Y. Wang, D. A. Muller, L. W. Martin, P. Hu, X. Zhang, *Phys. Rev. Lett.* **2018**, *120*, 227601.
[58] C. Cui, W.-J. Hu, X. Yan, C. Addiego, W. Gao, Y. Wang, Z. Wang, L. Li, Y. Cheng, P. Li, X. Zhang, H. N. Alshareef, T. Wu, W. Zhu, X. Pan, L.-J. Li, *Nano Lett.* **2018**, *18*, 1253.
[59] B. Lv, Z. Yan, W. Xue, R. Yang, J. Li, W. Ci, R. Pang, P. Zhou, G. Liu, Z. Liu, W. Zhu, X. Xu, *Mater. Horiz.* **2021**, *8*, 1472.
[60] M. Abes, C. T. Koops, S. B. Hrkac, J. McCord, N. O. Urs, N. Wolff, L. Kienle, W. J. Ren, L. Bouchenoire, B. M. Murphy, O. M. Magnussen, *Phys. Rev. B* **2016**, *93*, 195427.
[61] E. R. Callen, H. B. Callen, *Phys. Rev.* **1963**, *129*, 578.
[62] S. Yang, X. Ren, *Phys. Rev. B* **2008**, *77*, 014407.
[63] A. Lisfi, C. M. Williams, L. T. Nguyen, J. C. Lodder, A. Coleman, H. Corcoran, A. Johnson, P. Chang, A. Kumar, W. Morgan, *Phys. Rev. B* **2007**, *76*, 054405.
[64] F. Kronast, S. V. Molina, *J. Large-Scale Res. Facilit.* **2016**, *2*, A90.
[65] A. Sander, G. Orfila, D. Sanchez-Manzano, N. Reyren, M. A. Mawass, F. Gallego, S. Collin, K. Bouzehouane, K. Höflich, F. Kronast, F. Grilli, A. Rivera-Calzada, J. Santamaria, J. E. Villegas, S. Valencia, *Sci. Rep.* **2021**, *11*, 20788.
[66] S. M. Neumayer, S. Saremi, L. W. Martin, L. Collins, A. Tselev, S. Jesse, S. V. Kalinin, N. Balke, *J. Appl. Phys.* **2020**, *128*, 171105.
[67] S. Hong, *J. Appl. Phys* **2021**, *129*, 051101.
[68] A. Gruverman, M. Alexe, D. Meier, *Nat. Commun.* **2019**, *10*, 1661.
[69] P. Giannozzi, S. Baroni, N. Bonini, M. Calandra, R. Car, C. Cavazzoni, D. Ceresoli, G. L. Chiarotti, M. Cococcioni, I. Dabo, A. D. Corso, S. de Gironcoli, S. Fabris, G. Fratesi, R. Gebauer, U. Gerstmann, C. Gougoussis, A. Kokalj, M. Lazzeri, L. Martin-Samos, N. Marzari, F. Mauri, R. Mazzarello, S. Paolini, A. Pasquarello, L. Paulatto, C. Sbraccia, S. Scandolo, G. Sclauzero, A. P. Seitsonen, et al., *J. Condens. Matter Phys.* **2009**, *21*, 395502.
[70] W. Kohn, L. J. Sham, *Phys. Rev.* **1965**, *140*, A1133.
[71] G. Pizzi, V. Vitale, R. Arita, S. Blügel, F. Freimuth, G. Géranton, M. Gibertini, D. Gresch, C. Johnson, T. Koretsune, J. Ibañez Azpiroz, H. Lee, J.-M. Lihm, D. Marchand, A. Marrazzo, Y. Mokrousov, J. I. Mustafa, Y. Nohara, Y. Nomura, L. Paulatto, S. Poncé, T. Ponweiser, J. Qiao, F. Thöle, S. S. Tsirkin, M. Wierzbowska, N. Marzari, D. Vanderbilt, I. Souza, A. A. Mostofi, et al., *J. Phys.: Condens. Matter* **2020**, *32*, 165902.
[72] X. He, N. Helbig, M. J. Verstraete, E. Bousquet, *Comput. Phys. Commun.* **2021**, *264*, 107938.
[73] R. F. L. Evans, W. J. Fan, P. Chureemart, T. A. Ostler, M. O. A. Ellis, R. W. Chantrell, *J. Condens. Matter Phys.* **2014**, *26*, 103202.